A *Swift* view on IGR J19149+1036

G. Cusumano,[1]⋆ A. Segreto,[1] V. La Parola,[1] N. Masetti,[2] A. D'Aì and G. Tagliaferri[3]

[1]*INAF - Istituto di Astrofisica Spaziale e Fisica Cosmica, Via U. La Malfa 153, I-90146 Palermo, Italy*
[2]*INAF - Istituto di Astrofisica Spaziale e Fisica Cosmica di Bologna, via Gobetti 101, I-40129 Bologna, Italy*
[3]*INAF - Brera Astronomical Observatory, via Bianchi 46, I-23807 Merate (LC), Italy*

ABSTRACT

IGR J19149+1036 is a high-mass X-ray binary detected by *INTEGRAL* in 2011 in the hard X-ray domain. We have analysed the Burst Alert Telescope (BAT) survey data of the first 103 months of the *Swift* mission detecting this source at a significance level of ∼30 standard deviations. The timing analysis on the long-term BAT light curve reveals the presence of a strong sinusoidal intensity modulation of 22.25 ± 0.05 d, that we interpret as the orbital period of this binary system. A broad-band (0.3–150 keV) spectral analysis was performed combining the BAT spectrum and the X-Ray Telescope (XRT) spectra from the pointed follow-up observations. The spectrum is adequately modelled with an absorbed power law with a high-energy cutoff at ∼24 keV and an absorption cyclotron feature at ∼31 keV. Correcting for the gravitational redshift, the inferred magnetic field at the neutron star surface is $B_{surf} \sim 3.6 \times 10^{12}$ G.

Key words: X-rays: binaries – X-rays: individual: IGR J19149+1036.

1 INTRODUCTION

Since 2004 November, the Burst Alert Telescope (BAT; Barthelmy et al. 2005) on board the *Swift* observatory (Gehrels et al. 2004) has been scanning the entire sky in the hard X-ray domain (15–150 keV) recording timing and spectral information for any detected source (more than 1700 sources after 100 months of survey[1]). Thanks to its wide field of view and to the *Swift* pointing strategy, the BAT observes daily ∼90 per cent of the sky, and therefore it is specially fit for source variability studies. BAT has proved to be a valuable tool to detect transient phenomena from known and unknown sources (Krimm et al. 2013) and, by combining the entire data span, to reveal long periodicities of Galactic high-mass X-ray binaries (HMXB, e.g. Corbet & Krimm 2009, 2010; Corbet, Krimm & Skinner 2010a; Corbet et al. 2010b,c,d,e; Cusumano et al. 2010, 2013a,b; La Parola et al. 2010, 2013; D'Aì et al. 2011a; Segreto et al. 2013a,b).

In this paper, we present a comprehensive temporal and spectral analysis of the *Swift* data collected on IGR J19149+1036. This source was detected by IBIS/ISGRI at a position consistent with the *Einstein* source 2E 1912.5+1031 (Pavan et al. 2011), although a firm association was not possible due to large systematic uncertainties related to the presence of GRS 1915+105 at a distance lower than ∼20 arcmin. The source was also detected by *JEM-X* with a 3–10 keV X-ray flux of 7×10^{-12} erg s^{-1} cm^{-2}. The field around IGR J19149+1036 was observed by *Swift*/X-Ray Telescope (XRT) several times. The anal-

ysis of the XRT data collected on 2010 December 5 and 2011 February 17, reported in Bozzo et al. (2011), allowed us to estimate a refined source position at RA = $19^h 14^m 56\overset{s}{.}73$ and Dec = $+10°36'38\overset{''}{.}11$ (J2000), with an associated uncertainty of 3.7 arcsec, that confirmed the association with 2E 1912.5+1031 suggested by Pavan et al. (2011). The XRT spectrum was modelled by an absorbed power law with a column density $N_H = 6.5 \times 10^{22}$ cm^{-2} and a photon index $\Gamma = 1.8$, with an observed 1–10 keV X-ray flux of 1.8×10^{-11} erg s^{-1} cm^{-2}. 2MASS J19145680+1036387 ($J = 14.34$, $H = 12.41$, $K = 11.53$), within the XRT error circle, is the most likely counterpart to IGR J19149+1036.

This paper is organized as follows. Section 2 describes the BAT and XRT data reduction. Section 3 reports on the timing analysis. Section 4 describes the broad-band spectral analysis. In Section 5, we briefly discuss our results.

2 OBSERVATIONS AND DATA REDUCTION

The results reported in this paper on IGR J19149+1036 derive from the analysis of the BAT survey data relevant to the first 103 months of the *Swift* mission. The data were retrieved from the *Swift* public archive[2] in the form of detector plane histograms (DPH): three-dimensional arrays (two spatial dimensions, one spectral dimension) that collect count rate data in 5-min time bins for 80 energy channels. We use a dedicated software (Segreto et al. 2010) to process these data, producing all-sky maps in several energy intervals between 15 and 150 keV, detecting sources on these maps and extracting, for each source, standard products such as light curves and

⋆ E-mail: cusumano@ifc.inaf.it
[1] http://bat.ifc.inaf.it

[2] http://heasarc.gsfc.nasa.gov/cgi-bin/W3Browse/swift.pl

spectra. Fig. 1 (top panel) shows the 15–150 keV significance sky map (exposure time 39.4 Ms) in the direction of IGR J19149+1036. The source is close (∼20 arcmin) to the much brighter object GRS 1915+105: the positions of these two sources are marked with black crosses. In this map IGR J19149+1036 is not immediately detected because it is embedded in the point spread function (PSF) signal of the close brighter source. However, if we extract the values of the significance along the line that connects the optical position of the two sources (magenta line in the top panel of Fig. 1) we observe an asymmetric profile (Fig. 1, central panel) that suggests the presence of a faint source (IGR J19149+1036) hidden by the PSF of the brighter one (GRS 1915+105). Indeed, the fit of this profile with a single Gaussian shows systematic residuals; conversely, the profile is well fitted with a double Gaussian. The best-fitting peaks of the two Gaussians correspond to the position of the two sources. In order to make IGR J19149+1036 emerge in the sky map, we perform on each DPH a subtraction of the expected illumination pattern from all the detected sources; from the resulting 'residual shadowgrams' we generate new survey 'residual maps' where any previously undetected source can emerge. IGR J19149+1036 was detected in the 15–150 keV all-sky 'residual map' (Fig. 1, bottom panel) with a signal-to-noise ratio (S/N) of 28.6 standard deviations and of 31.7 standard deviations in the 15–60 keV all-sky map, where its S/N is maximized. The 15–60 keV energy band was used to extract the light curve with the maximum resolution (∼300 s) allowed by the *Swift*-BAT survey data. For each time bin the contribution from GRS 1915+105 is subtracted. The time tag of each bin, defined as the central time of the bin interval, was corrected to the Solar system barycentre (SSB) by using the task EARTH2SUN. The background subtracted spectrum averaged over the entire survey period was extracted in 14 energy channels and analysed using the BAT redistribution matrix available in the *Swift* calibration data base.[3]

Swift-XRT (Burrows et al. 2004) observed the field around IGR J19149+1036 five times after the discovery of the source by *INTEGRAL*. The source was always observed in Photon Counting (PC) mode (Hill et al. 2004) for a total exposure of ∼3800 s. The details on the five *Swift*-XRT observations are reported in Table 1. The XRT data were processed with standard procedures (XRTPIPELINE v.0.12.8) using the FTOOLS in the HEASOFT package (v 6.15) and the products were extracted adopting a grade filtering of 0–12. The source events for timing and spectral analysis were extracted from a circular region of 20 pixel radius (1 pixel = 2.36 arcsec) centred on the source position as determined with XRTCENTROID (RA = $19^h14^m56{.}8$ and Dec. = $+10°36'39{.}1$, J2000), while the background was extracted from an annular region centred on the source, with an inner radius of 60 pixels and an outer radius of 90 pixels that avoids contamination due to the stray-light from GRS J1915+105 and to the PSF tail of IGR J19149+1036. All source event arrival times were converted to the SSB with the task BARYCORR.[4] Ancillary response files were generated with XRTMKARF.[5] We also extracted a single source and a single background spectra from the five XRT observations and combined the relevant ancillary files using ADDARF, that weights them by the exposure times of the corresponding source spectra. Finally, the spectra were re-binned with a minimum of 20 counts per energy channel. This lower limit of counts per bin is enough to ensure that the deviation of the observed number of counts from the expected values approximates quite well a Gaussian distribution, that is a requirement to apply the
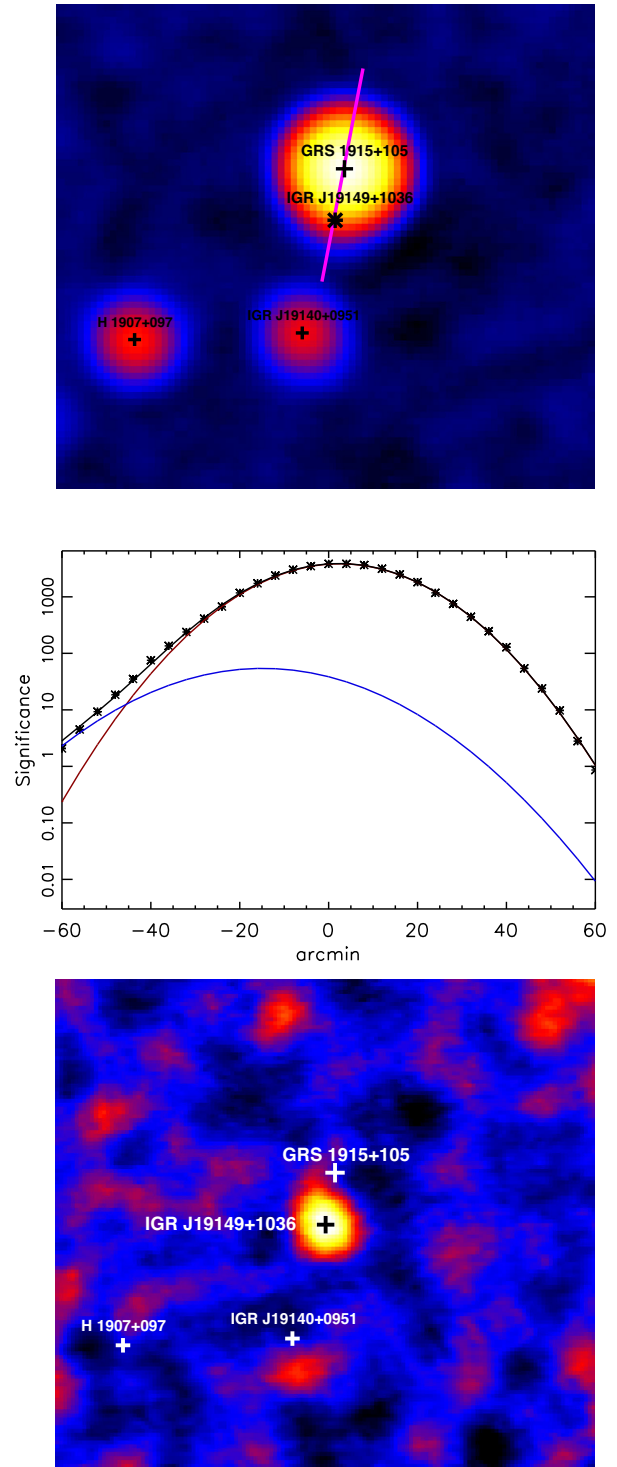
[3] http://swift.gsfc.nasa.gov/docs/heasarc/caldb/swift/
[4] http://heasarc.gsfc.nasa.gov/ftools/caldb/help/barycorr.html
[5] http://heasarc.gsfc.nasa.gov/ftools/caldb/help/xrtmkarf.html

Figure 1. Top panel: 15–150 keV BAT sky map around IGR J19149+1036. The crosses mark the position of the sources detected in the field; the star marks the XRT position of IGR J19149+1036. Middle panel: values of the significance extracted along the line that connects the optical position of the two sources (magenta line in the top panel). The plot shows the data (crosses) and the best-fitting model (black line, the sum of two Gaussian profiles). The higher peak (red line) corresponds to GRS 1915+105 while the lower peak (blue line) corresponds to IGR J19149+1036. Bottom panel: 15–150 keV significance 'residual map'.

Table 1. XRT observations log. The quoted orbital phase refers to the profile shown in Fig. 2.

Obs #	Obs ID	T_{start} MJD	$T_{elapsed}$ (s)	Exposure (s)	Rate (c s^{-1})	Orb. Phase
1	00041130001	55535.220	29 310.9	911.5	0.23 ± 0.02	0.47
2	00041130002	55609.162	46 002.1	1261.2	0.13 ± 0.01	0.79
3	00041130003	56267.370	388.6	387.1	0.13 ± 0.02	0.39
4	00041130004	56631.147	52911.4	849.1	0.10 ± 0.01	0.75
5	00067133005	56632.625	403.6	402.0	0.10 ± 0.02	0.81
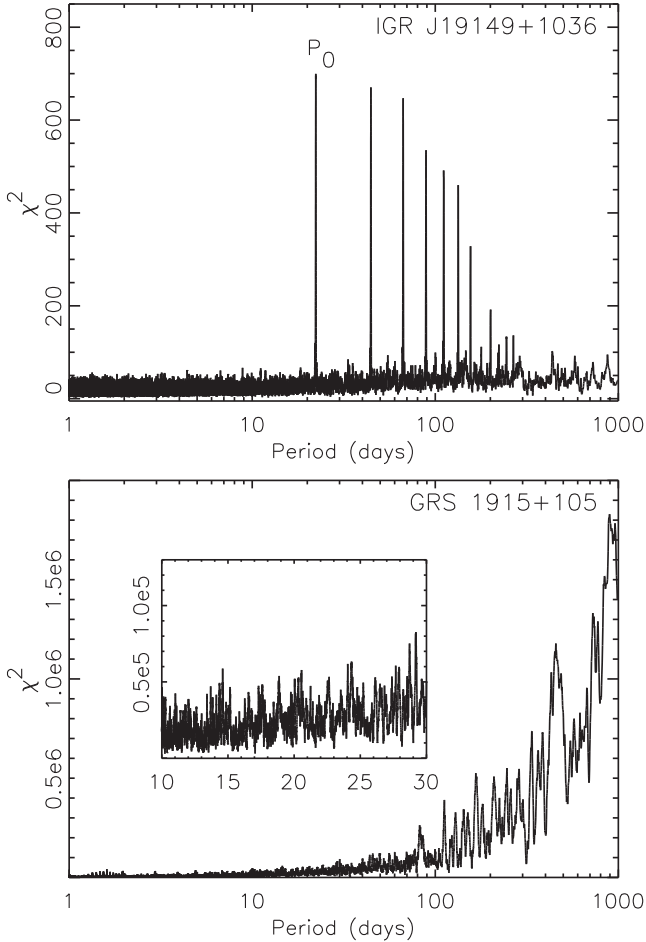
Figure 2. Top panel: periodogram of *Swift*-BAT (15–60 keV) data for IGR J19149+1036. Bottom panel: periodogram of *Swift*-BAT (15–60 keV) data for GRS 1915+105. The inset shows a close-up view of the periodogram in the 10–30 d interval.

χ^2 statistics. We used the spectral redistribution matrix v014 and the spectral analysis was performed using XSPEC v.12.5.

Errors are at 90 per cent confidence level for a single parameter, if not stated otherwise.

3 TIMING ANALYSIS AND RESULTS

We produced the periodogram of the long term *Swift*-BAT 15–60 keV light curve applying a folding technique (Leahy, Elsner & Weisskopf 1983) which consists in the production of a count rate profile at different trial periods by folding the photon arrival times in N phase bins and evaluating for each resulting profile the χ^2 value with respect to the average count rate. A periodic modulation corresponds to a large value of χ^2. We searched in the 1–1000 d

period range with a period spacing given by $P^2/(N \Delta T_{BAT})$ where P is the trial period, $N = 16$ and $\Delta T_{BAT} \sim 272.4$ Ms is the data span length. The average rate in each profile phase bin was evaluated by weighting the rates with the inverse square of their statistical error. This procedure is mandatory for data collected by a large field of view coded mask telescope as BAT that are characterized by a large spread of statistical errors. The periodogram (Fig. 2, top panel) shows the presence of several prominent features. The highest feature is at $P_0 = 22.25 \pm 0.05$ d ($\chi^2 \sim 702$) where P_0 and its error are the centroid and the standard deviation obtained by modelling this feature with a Gaussian function. Using the method described in Cusumano et al. (2013a), we find that the probability of finding such a high χ^2 value by chance is $\sim 10^{-58}$. The other features clearly visible in the periodogram and showing decreasing χ^2 peaks towards higher trial periods correspond to a series of multiples of P_0. We verified that the detected periodicity is not present in the periodogram of GRS 1915+105 as shown in the bottom panel of Fig. 2.

The intensity profile (Fig. 3, top panel) folded at P_0 with $T_{epoch} = 54924.32$ MJD is characterized by a single symmetric peak with a minimum consistent with zero intensity. The minimum dip centroid, evaluated by fitting the data with a Gaussian function, falls at phase 1.06 ± 0.01, corresponding to MJD $(54925.7 \pm 0.2) \pm n \times P_0$. The peak centroid is at phase 0.56 ± 0.01, corresponding to MJD $(54936.8 \pm 0.2) \pm n \times P_0$.

Fig. 3 (bottom panel) shows the 103 months BAT light curve with a time resolution of P_0 d. The source shows a quite persistent behaviour without any significant intensity enhancements, which is consistent with the very low-level of red noise observed in the source periodogram shown in Fig. 3, top panel.

Table 1 lists the average count rate during each XRT observation and the relevant orbital phase evaluated with respect to P_0 and T_{epoch}. We performed a timing analysis on the XRT data searching for the presence of a periodic modulation tied to the compact object rotation. In order to avoid systematics caused by the readout time in PC mode (characterized by a time resolution bin of $\delta T_{XRT} = 2.5073$ s), the arrival times of the events in PC mode were randomized within δT_{XRT}. Moreover, XRT observations are fragmented into snapshots of different duration and time separation that may introduce spurious features in the timing analysis. To avoid these systematics we performed a folding analysis on each snapshot with an exposure time higher than 500 s and with a statistical content larger than 100 counts, searching in a period range [δT_{XRT} : 100] s. The periodograms obtained from snapshots belonging to the same observation were also summed together. We did not found significant features in any of the resulting periodograms.

4 SPECTRAL ANALYSIS

Because the XRT and BAT data are collected at different times and with different exposures, we verified that no significant spectral
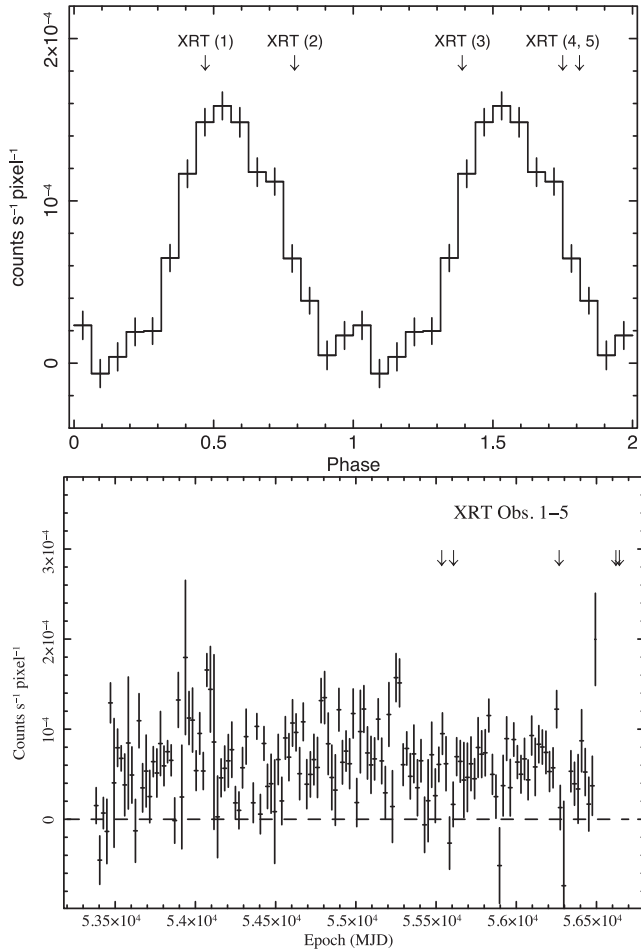
Figure 3. Top panel: *Swift*-BAT light curve folded at a period $P = 22.25 \pm 0.05$ d, with 16 phase bins. The arrow points to the phase corresponding to the time of the five XRT observations. Bottom panel: BAT light curve. The bin length corresponds to a time interval of P_0 d.

variability is present both among the five XRT observations and during the BAT monitoring. To this aim we produced hardness ratios of the source events in the energy bands 4–10 keV/0.5–4 keV from each XRT observation and in the energy bands 35–150 keV/15–35 keV for the BAT data. In both cases, no significant variability is observed.

In order to maximize the S/N of the BAT data, we produced a spectrum selecting the data in the phase interval 0.3–0.8 (see Fig. 3, top panel). Then fitted the BAT spectrum and the XRT spectrum obtained from the entire XRT data set using a common spectral model, including a multiplicative factor that is frozen to unity for the XRT spectrum and is left free to vary for the BAT spectrum, to account for any inter-calibration uncertainty between the two telescopes and/or for different average source intensity between the XRT and BAT observing times. The combined XRT-BAT spectrum (Fig. 4, top panel) was first modelled with an absorbed power law (model 1 `cons*phabs*powerlaw`) with a χ^2 of 74.7 with 34 degrees of freedom (d.o.f.). We also tried to model the broad-band spectrum including a cutoff in the model (model 2 `cons*phabs*cutoffpl`) obtaining a χ^2 of 69.9 (33 d.o.f.). Both models result indeed unacceptable, with residuals (Fig. 4, middle panel) that show a broad range residual pattern both in the XRT and in the BAT data. We
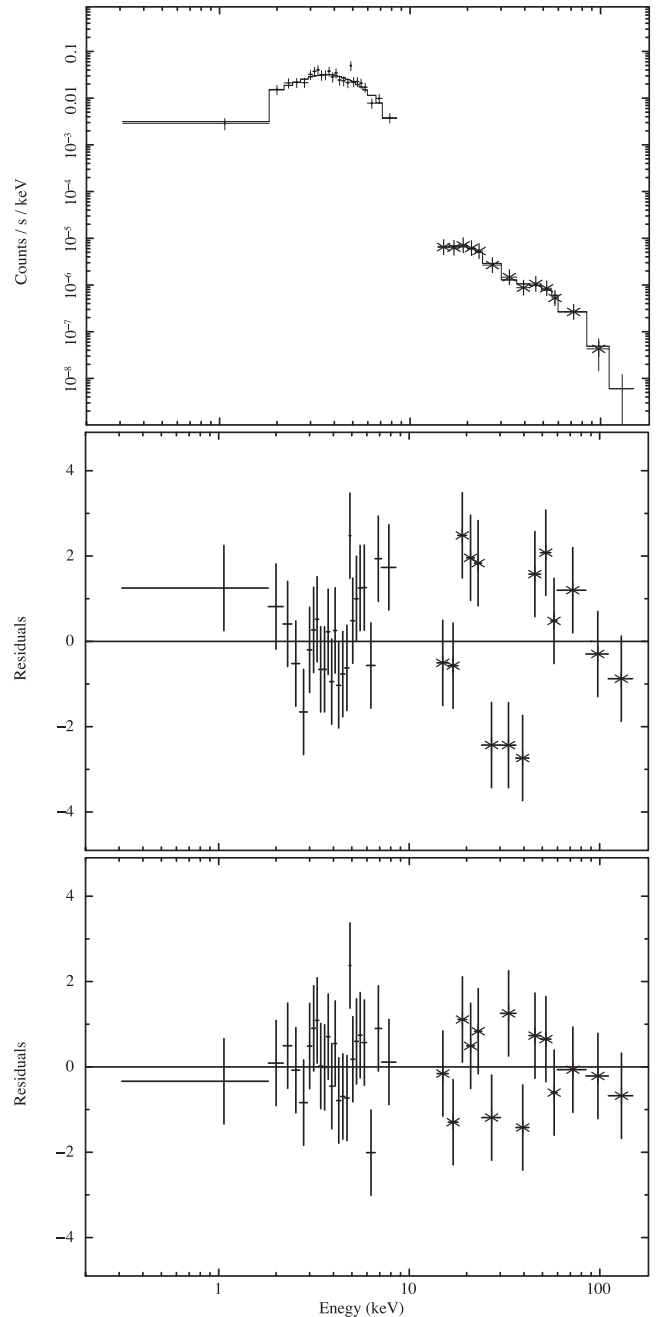

Figure 4. Top panel: IGR J19149+1036 XRT and BAT spectra and best-fitting `phabs*cutoffpl` model. Middle panel: residuals in unit of standard deviations for the `phabs*cutoffpl` model. Bottom panel: residuals in unit of standard deviations for the `phabs*cutoffpl*cyclabs` model.

added to both models an absorption cyclotron line (`cyclabs`), obtaining a significant improvement in the χ^2 (28.4, 30 d.o.f., with $\Delta\chi_0^2 = 41.5$) only for model 2 with a flat residual distribution (Fig. 4, bottom panel). Table 2 reports the spectral results of the best-fitting model. To estimate the statistical significance of the presence of the cyclotron absorption feature we applied a Monte Carlo simulation on the BAT spectrum. The details of this procedure can be found in D'Aì et al. (2011b). We find that the probability of chance occurrence to find a $\Delta\chi^2$ value ≥ 41.5 is $\sim 2.7 \times 10^{-6}$.

Table 2. Best-fitting spectral parameters for the `phabs*cutoffpl*cyclabs` model. C_{BAT} is the constant factor to be multiplied to the model in order to match the XRT and BAT data. We report observed fluxes for the standard XRT (0.3–10 keV) and BAT (15–150 keV) energy bands.

Parameter	Best-fitting value	Units
n_H	$3.9^{+0.3}_{-0.1} \times 10^{22}$	cm^{-2}
Γ	$0.9^{+0.4}_{-0.4}$	
E_{cut}	24^{+10}_{-5}	keV
N	$1.8^{+1.6}_{-0.8} \times 10^{-3}$	ph keV^{-1}cm^{-2} s^{-1} at 1 keV
C_{BAT}	$1.1^{+0.5}_{-0.4}$	
E_{cyc}	$31.2^{+1.9}_{-2.2}$	keV
D_{cyc}	$0.9^{+0.4}_{-0.4}$	
W_{cyc}	$8.4^{+4.2}_{-2.8}$	keV
F (0.3–10 keV)	1.76×10^{-11}	erg s^{-1} cm^{-2}
F (15–150 keV)	4.53×10^{-11}	erg s^{-1} cm^{-2}
χ^2	28.4 (30 d.o.f.)	

5 CONCLUSIONS

We have analysed the *Swift*-BAT and XRT data relevant to the HMXB IGR J19149+1036. The source is close ($\sim$20 arcmin) to the much brighter source GRS 1915+105, and an ad hoc imaging analysis was necessary to reveal it in the BAT all sky map, where it emerges at a significance level of $\sim$29 ($\sim$32) standard deviations in the 15–150 keV (15–60 keV) band after 103 months of the *Swift* mission. The timing analysis on the long-term BAT light curve unveils the presence of a periodic modulation in the hard X-ray emission with a period of $P_0 = 22.25 \pm 0.05$ d. We interpret this modulation as the orbital period of the binary system. The folded light curve is characterized by a single symmetric peak with a roughly sinusoidal shape that shows a minimum consistent with zero intensity, lasting $\sim$30 per cent of the orbital period. Such a long minimum intensity phase interval is difficult to explain with a full eclipse of the compact object, unless we speculate that the system has both an extremely eccentric orbit and a high inclination angle. An alternative explanation is that the modulation is caused by the passage of the compact source through the stellar wind, whose density decreases as the source approaches the orbit apastron. However, no definite conclusion on the geometry of the binary system can be drawn, without knowing the spectral type of the companion star.

The broad-band spectrum cannot be adequately described by the standard continua used for HMXB, because of the presence of an absorption feature within the BAT energy range. We obtain a good description of the data introducing a cyclotron line in the cutoff power-law model. The energy of the cutoff is $\sim$24 keV and the line is centred at $E_{cyc} \sim 31$ keV. The presence of absorption cyclotron lines has been revealed in several HMXB. They are thought to be originated near the magnetic poles of the neutron star due to resonant scattering processes of the X-rays by electrons whose kinetic energies are quantized in discrete Landau energy levels perpendicular to the B-field (Schönherr et al. 2007). Their energy centroid is related to the intensity of the magnetic field of the neutron star:

$$B_{obs} = 10^{12} \times \frac{E_{cyc}/(1 \text{ keV})}{11.6} \text{ G} \sim 2.7 \times 10^{12} \text{ G}. \quad (1)$$

If the cyclotron absorption takes place near the poles of the neutron star the observed resonance energy shall be corrected by the effect of the gravitational redshift: $E_{cyc}^{obs} = E_{cyc}(1 + z)^{-1}$ with

$$(1 + z)^{-1} = \left(1 - \frac{2GM_{ns}}{R_{ns}c^2} \right)^{0.5}. \quad (2)$$

Using standard parameters for the neutron star ($M_{ns} = 1.4 \, M_\odot$, $R_{ns} = 10^6$ cm), the magnetic field at the neutron star surface would be $B_{surf} \sim 3.6 \times 10^{12}$ G. This result is fully consistent with the distribution of the magnetic field values derived for neutron stars in binary systems, that peaks in the range 1–4 $\times 10^{12}$ G (Makishima et al. 1999).

REFERENCES

Barthelmy S. D. et al., 2005, Space Sci. Rev., 120, 143
Bozzo E., Ferrigno C., Pavan L., Walter R., Stella L., 2011, Astron. Telegram, 3326, 1
Burrows D. N. et al., 2004, Proc. SPIE, 5165, 201
Corbet R. H. D., 1986, MNRAS, 220, 1047
Corbet R. H. D., Krimm H. A., 2009, Astron. Telegram, 2008, 1
Corbet R. H. D., Krimm H. A., 2010, Astron. Telegram, 3079, 1
Corbet R. H. D., Krimm H. A., Skinner G. K., 2010a, Astron. Telegram, 2559, 1
Corbet R. H. D., Krimm H. A., Barthelmy S. D., Baumgartner W. H., Markwardt C. B., Skinner G. K., Tueller J., 2010b, Astron. Telegram, 2570, 1
Corbet R. H. D., Barthelmy S. D., Baumgartner W. H., Krimm H. A., Markwardt C. B., Skinner G. K., Tueller J., 2010c, Astron. Telegram, 2588, 1
Corbet R. H. D. et al., 2010d, Astron. Telegram, 2598, 1
Corbet R. H. D., Barthelmy S. D., Baumgartner W. H., Krimm H. A., Markwardt C. B., Skinner G. K., Tueller J., 2010e, Astron. Telegram, 2599, 1
Cusumano G., La Parola V., Romano P., Segreto A., Vercellone S., Chincarini G., 2010, MNRAS, 406, L16
Cusumano G., Segreto A., La Parola V., Masetti N., D'Aì A., Tagliaferri G., 2013a, MNRAS, 436, L74
Cusumano G., Segreto A., La Parola V., D'Aì A., Masetti N., Tagliaferri G., 2013b, ApJ, 775, L25
D'Aì A., La Parola V., Cusumano G., Segreto A., Romano P., Vercellone S., Robba N. R., 2011a, A&A, 529, A30
D'Aì A., Cusumano G., La Parola V., Segreto A., di Salvo T., Iaria R., Robba N. R., 2011b, A&A, 532, A73
Gehrels N. et al., 2004, ApJ, 611, 1005
Hill J. E. et al., 2004, Proc. SPIE, 5165, 217
Krimm H. A. et al., 2013, ApJS, 209, 14
La Parola V., Cusumano G., Romano P., Segreto A., Vercellone S., Chincarini G., 2010, MNRAS, 405, L66
La Parola V., Cusumano G., Segreto A., D'Aì A., Masetti N., D'Elia V., 2013, ApJ, 775, L24
Leahy D. A., Elsner R. F., Weisskopf M. C., 1983, ApJ, 272, 256
Makishima K., Mihara T., Nagase F., Tanaka Y., 1999, ApJ, 525, 978

Pavan L., Bozzo E., Ferrigno C., Ricci C., Manousakis A., Walter R., Stella L., 2011, A&A, 526, A122

Schönherr G., Wilms J., Kretschmar P., Kreykenbohm I., Santangelo A., Rothschild R. E., Coburn W., Staubert R., 2007, A&A, 472, 353

Segreto A., Cusumano G., Ferrigno C., La Parola V., Mangano V., Mineo T., Romano P., 2010, A&A, 510, A47

Segreto A., Cusumano G., La Parola V., D'Aì A., Masetti N., D'Avanzo P., 2013a, A&A, 557, A113

Segreto A., La Parola V., Cusumano G., D'Aì A., Masetti N., Campana S., 2013b, A&A, 558, A99

This paper has been typeset from a T_EX/L^AT_EX file prepared by the author.